symmetry

MDPI

Article

A Machine Learning Strategy for the Quantitative Analysis of the Global Warming Impact on Marine Ecosystems

Hosam Alhakami [1,*], Mustafa Kamal [2], Muhammad Sulaiman [2,*], Wajdi Alhakami [3] and Abdullah Baz [4]

[1] Department of Computer Science, College of Computer and Information Systems, Umm Al-Qura University, Makkah 21955, Saudi Arabia
[2] Department of Mathematics, Abdul Wali Khan University, Mardan 23200, Pakistan
[3] Department of Information Technology, College of Computers and Information Technology, Taif University, Taif 26571, Saudi Arabia
[4] Department of Computer Engineering, College of Computer and Information Systems, Umm Al-Qura University, Makkah 21955, Saudi Arabia
* Correspondence: hhhakam@uqu.edu.sa (H.A.); msulaiman@awkum.edu.pk (M.S.)

Abstract: It is generally observed that aquatic organisms have symmetric abilities to produce oxygen (O_2) and fix carbon dioxide (CO_2). A simulation model with time-dependent parameters was recently proposed to better understand the symmetric effects of accelerated climate change on coastal ecosystems. Changes in environmental elements and marine life are two examples of variables that are expected to change over time symmetrically. The sustainability of each equilibrium point is examined in addition to proving the existence and accuracy of the proposed model. To support the conclusions of this research compared to other studies, numerical simulations of the proposed model and a case study are investigated. This paper proposes an integrated bibliographical analysis of artificial neural networks (ANNs) using the Reverse-Propagation with Levenberg–Marquaradt Scheme (RP-LMS) to evaluate the main properties and applications of ANNs. The results obtained by RP-LMS show how to prevent global warming by improving the management of marine fish resources. The reference dataset for greenhouse gas emissions, environmental temperature, aquatic population, and fisheries population (GAPF) is obtained by varying parameters in the numerical Adam approach for different scenarios. The accuracy of the proposed RP-LMS neural network is demonstrated using mean square error (MSE), regression plots, and best-fit output. According to RP-LMS, the current scenario of rapid global warming will continue unabated over the next 50 years, damaging marine ecosystems, particularly fish stocks.

Keywords: marine ecosystem; Levenberg–Marquardt method; numerical simulations; greenhouse gases; artificial neural network; machine learning

Citation: Alhakami, H.; Kamal, M.; Sulaiman, M.; Alhakami, W.; Baz, A. A Machine Learning Strategy for the Quantitative Analysis of the Global Warming Impact on Marine Ecosystems. *Symmetry* **2022**, *14*, 2023. https://doi.org/10.3390/sym14102023

Academic Editor: Juan Luis García Guirao

Received: 15 August 2022
Accepted: 19 September 2022
Published: 26 September 2022

1. Introduction

The struggle between living organisms and their environment is a universal phenomenon. Since the agricultural revolution, emissions of greenhouse gases into the atmosphere have increased rapidly [1–3]. The global climate is constantly changing as the concentration of greenhouse gases increases. They mostly affect marine ecosystems as a result of acidification, warming, and natural disasters (floods, tsunamis, and so on) [4–12]. The release of extreme greenhouse gases has serious irreversible consequences in the form of climate change and rising temperatures. According to scientists, around 83% of greenhouse gases are produced, and climate change is primarily caused by human activity. Extreme global warming concentrations are causing a rapid rise in sea levels. The average (CO_2) concentration continued to rise, from 280.01 to 380.01 (ppmv). Examine the last 0.8 million years of history.

Aquatic organisms are speculated to be the most important oxygen (O_2) producers and carbon dioxide (CO_2) absorbers. Through the transportation of energy, high temperatures, and nutrients, marine ecosystems play an important role in balancing ecological change. For example, marine ecosystems act as carbon dioxide sinks, which actually reduces the rate of global warming. Climate change, which is a source of O_2 since phytoplankton produces nearly 70% of O_2 [13,14], is also a source of proteins and vitamins for humans [15–17]. In general, rapid global warming has a negative effect on the number of greenhouse gases in the atmosphere. This makes it harder for marine phytoplankton, fish, and algae to grow [5–7]. Numerous studies have been published on the consequences of global climate change on the biodiversity of coastal and marine habitats [18–21].

Moreover, numerous studies [22–24] provide statistical explanations for the probable consequences of climate change on marine coastal biodiversity. A companion article estimates the effects of climate change on a specific coastal area using mathematical approaches. Hiners et al. [25] developed an accurate model to investigate the effects of global climate change on marine aquatic plants and discovered that the rate of evolution of marine plankton differs from that of climate change. Schercher and Petrovski [13] investigated the impact of saturation (CO_2) on maritime trophic evolution and concluded that it is faster compared to the oceans (CO_2). Speers et al. [8] demonstrated how degradation and climate change damage aquatic marine biodiversity, particularly coral reefs and fish habitats. Through statistical analysis, they found that almost 92 percent of marine sea creatures may be gone by the end of the year 2100. However, those studies do not specify how or how much the density of marine species will vary as a result of any environmental change. The authors of that research established mathematically and empirically that the consequences of global warming continue to harm entire ecosystems, and that if this scenario continues, 80–90 percent of the diversity of ecological systems could be lost by the end of this century. The effects of climate change on the coastal habitats of the Pacific Ocean were scientifically examined by Asch et al. [10]. The most current analysis distinguishes each of these contributions as a component of the marine ecosystem, and Table 1 makes this distinction quite evident. A set of nonlinear ordinary differential Equation (1) serves as the foundation for the model. The reference dataset for greenhouse gas emissions, environmental temperature, aquatic population, and fisheries population (GAPF) is obtained by modifying the parameters of the NDSolve techniques for various scenarios. Using Equation (1) from 0 to 50 intervals with a 0.04 step size, a reference dataset of 1251 points is generated for each GAPF model scenario.

The GAPF model has previously been studied using various analytical methods; however, the stochastic mathematical processing tool dealing with RP-LMS has recently been used to analyze GAPF. Due to their successful applications in numerous technical and scientific fields, such as sustainable-security assessment [26] digital logic [27], image recognition [28], electronic systems [29], computational intelligence [30], and analog thinking [31], to name just a few, artificial neural networks (ANNs) have emerged as an innovative alternative to mimic systems. Fluid Mechanics [32–37], Biomedicine [38–40], Financial and Business Systems [41,42], Engineering Application [43], Physics of Fluids [43], Models of Panto-Graph Delay Differential Systems [44], and other interesting ones. Research papers have all benefited from the accurate results provided by stochastic numerical calculations. All these motivating features encourage researchers to use an AI algorithm-based numerical computational model for the numerical exploration model, combining graphical and numerical analysis to predict the future of the coastal environment (algae and freshwater bodies) in the face of the rapid investigation of global warming. The research is divided into many steps, which are summarized below.

- The RP-LMS neural network is a novel supervised computational paradigm that we designed. It is fast and efficient and requires little computing power.
- For the GAPF model, the original mathematical equations are solved by the RK4 method to prepare the dataset for the RP-LMS neural network. For the convenience of readers, the notations used in this paper are summarized in the abbreviation section.

- The presentation of the designed neural network through RP-LMS for successfully resolving the GAPF model was further validated by mean square error, regression analysis, and histogram convergence plot.
- The correctness and repeatability of the design schemes were further validated using reliability, effectiveness, MSE convergence analysis, correlation analysis, and bar charts.
- Table 1 gives a quick summary of some relevant studies conducted in the past and illustrates how they differ from the suggested approach (RP-LMS).

Table 1. Previous studies compared to this study.

Literature Review	Parameter Growth Rate of Growth and Rate of Decline		Effect of Climate Change on Marine Ecosystem			Solution Type		Case Study
	Secondary	Measured	Global Warming	Marine Plankton	Fish Community	Exact	Heuristic	
Hinners et al. [25]	Yes	No	Yes	Yes	No	Yes	No	No
Asch et al. [10]	Yes	No	Yes	Yes	Yes	No	No	No
Mandal et al. [16]	No	Yes	Yes	Yes	No	Yes	No	No
Speers et al. [8]	Yes	No	Yes	Yes	Yes	Yes	No	No
Sekerci and Petrovskii [13]	No	Yes	Yes	Yes	No	Yes	No	No
This study	No	Yes	Yes	Yes	Yes	Yes	Yes	Yes

2. Mathematical Formulation

The study aims to find out how global warming affects aquatic ecosystems. Due to the rapid emission of greenhouse gases (plankton and fish community), marine habitats are evaluated in the context of global warming. Environmental phenomena are identified using mathematical models. Heterogeneous processes are divided into four categories, the number of greenhouse gases released into the atmosphere W(t) originating from different (but comparable) sources (slow human activity and natural phenomena) [1], an increase in atmospheric temperature X(t), which leads to a high concentration of carbon dioxide in the environment and is responsible for the greenhouse effect Y(t), and fish density in marine ecosystems decreases with altitude due to rapid temperature rise, salinity, oxygen starvation, and plankton population depletion Z(t). Figure 1 shows a schematic diagram of the model showing how anthropogenic climate change and greenhouse gas concentrations affect ocean life. The following mathematical model, which is made up of a series of NODEs, was recently proposed:

$$\begin{cases} \frac{dW}{dt} = n_1 W + \Delta_1 ZW - \Delta_2 YW - \Delta_3 X, \\ \frac{dX}{dt} = n_2 X + \psi_1 WX - \psi_2 YX, \\ \frac{dY}{dt} = n_3 Y(1 - \frac{Y}{A_1}) + \chi_1 Y - \chi_2 YX - \chi_3 ZY - \chi_4 WY, \\ \frac{dZ}{dt} = n_4 Z(1 - \frac{Z}{A_2}) + \beta_1 YZ - \frac{\beta_2 Z}{\alpha + W} - \beta_3 XZ. \end{cases} \tag{1}$$

with initial conditions
$W_0 = W(0) > 0, \;\; X_0 = X(0) > 0,$
$Y_0 = Y(0) \geq 0, \;\; Z_0 = Z(0) \geq 0,$

Four different categories are depicted in Figure 1.

1. Greenhouse gases that contribute to global warming W(t)
2. Atmospheric temperature X(t)
3. Planktonic individuals Y(t)
4. The Fishing Community Z(t).

The rates at which different factors (mostly human activities and, over time, physical processes) change the number of greenhouse gases released into the atmosphere are represented by Z(t) and W(t). X(t) is the high ambient temperature, which rises steadily with the maximum absorption of ecological GHGs and causes global warming. Y(t) is the strength of the planktonic community in the coastal environment, which is constantly threatened by the effects of climate change. In the presence of UV radiation, environmental gases undergo several chemical reactions. During the reaction phase, they give off energy, which raises the temperature of the environment and makes a number of new GHG components that add to the amount of GHGs in the atmosphere. Here, n_1 and n_2 represent typical growth rates, respectively. Alternatively, n_3 and n_4 are the typical growth rates of Y(t) and Z(t) in the absence of negative effects from GHGs and climate change. In maritime zones, Plankton (phytoplankton) absorbs carbon dioxide for respiration, and reducing the number of greenhouse gases in the air. ϕ_1 represents the rise in GHG intensity caused by the marine fish, while ϕ_2 represents the planktonic population's absorption of ambient GHGs whereas ϕ_3 represents the emission of greenhouse gases as a result of global warming.

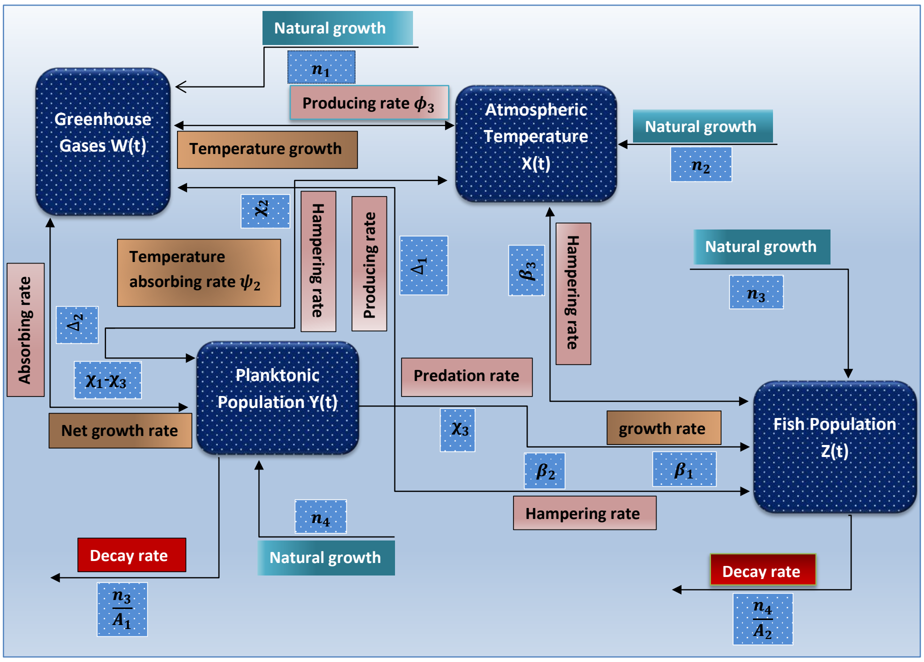

Figure 1. Schematic diagram of Model (1) showing the effect of greenhouse gas on temperature rise and the effect on marine environment and fishing community [16].

The environmental temperature increases accordingly to the quantity of ambient GHGs, such as Δ_1, which represents the rise in atmospheric temperature caused by the increase in GHGs. Temperature is a crucial component in marine plankton photosynthesis (phytoplankton). Thus, through photosynthesis, the quantity of maritime phytoplankton population can moderate the temperature rise. Here, Δ_2 represents the ambient temperature absorbed by the planktonic population. We consider A_1 and A_2 to be the sustaining capabilities of the prokaryotes and fishery communities, respectively, with the associated decay rates $\frac{n_3}{A_1}$ and $\frac{n_4}{A_2}$. Although the density of dispersed $CO2$ promotes the concentration of maritime phytoplankton, when the density of dissolved $CO2$ is so high, it limits phytoplankton metabolism by lowering the volume of dissolved $O2$, which slows the growth of the aquatic community. The influence of saturated carbon dioxide and dissolved oxygen deficit limit the growth of marine fisheries. As a result, $chi1$ denotes the rise in planktonic inhabitants brought on by CO_2 absorption, chi_2 reflects the decline in planktonic inhabitants brought on by warming, chi_3 represents the improvement in planktonic inhabitants brought on by exploitation or expenditure of fishery resources, and chi_4 denotes the reduction in planktonic inhabitants brought on by acidity. While β_1 represents the number of fish that rise as a result of eating plankton, β_2 represents the number of fish that decrease amount of absorbed CO_2, and β_3 represents the number of fish that decrease due to climate change. Table 2 summarises the parametric descriptions as well as the related values.

Table 2. Describe the relevant values of the parameters used in this study.

Symbols	Descriptions	Values
n_1	GHG levels in the oceans are naturally growing.	0.00095 kg/km^2
n_2	Plankton-feeding fish growth during the period	0.099 °C
n_3	The normal rate of expansion of the aquatic species	0.00225 km^{-3}
n_4	The perfectly natural increase in the population of fish	0.0002/1000
Δ_1	The oceanic aquatic demographic's rate of GHG production	0.0029 kg/km^2
Δ_2	GHG absorption rate by planktonic populations in the oceans	0.00099 kg/km^2
Δ_3	Due to rising temperatures, the rate at which GHGs are emitted	1.0 µ kg/km^2
χ_1	Planktonic population growth rate due to CO_2	0.00108 km^{-3}
χ_2	Nutrient rates are slowing as a result of global warming	0.00001 km^{-3}
χ_3	The rate at which fish consume plankton.	0.0031 km^{-3}
χ_4	Effects of acidity on plankton loss	10.1 µ km^{-3}
ψ_1	GHG-induced increase in the rate of surface temperatures	0.00025 °C
ψ_2	Rate of temperature absorption by the planktonic community	0.00565 °C
β_1	Plankton feeding/consumption increases the growth rate of fish populations.	175 µ/1000
β_2	The fish population declines to owe to acidification caused by GHGs.	190 µ/1000
β_3	Global warming is slowing the growth of fish populations	61 µ/1000
α	Stability in the level of saturation	0.01
A_1	Planktonic population's capacity for sustained growth	1,000,000 km
A_2	The population's ability to sustain themselves	10,000 km

The (GAPT) model is discussed for three different scenarios by considering the parameters such as the absorption rate of greenhouse gases by the plankton population in oceans (Δ_1), inhibition rate of plankton as a consequence of climate change (Δ_2) and global climate change has a significant impact on fish populations (Δ_3). The variation of different parameters is clearly discussed in Table 3.

Table 3. Variation of the parameters in the case study.

Scenarios	Cases	Parameters Δ_1	Δ_2	Δ_3	χ_1	χ_2	χ_3	χ_4	β_1	β_2	β_3	α	ψ_1	ψ_2
1	**1**	0.0029	0.00101	1	0.0011	0.00001	0.0031	10.1	0.000000175	0.00000019	6.1×10^{-7}	0.01	0.00025	0.00565
	2	0.0029	0.00108	1	0.0011	0.00001	0.0031	10.1	0.000000175	0.00000019	6.1×10^{-7}	0.01	0.00025	0.00565
	3	0.0029	0.00114	1	0.0011	0.00001	0.0031	10.1	0.000000175	0.00000019	6.1×10^{-7}	0.01	0.00025	0.00565
2	**1**	0.0029	0.00099	1	0.0011	0.00001	0.0031	10.1	0.000000175	0.00000019	6.1×10^{-7}	0.01	0.00025	0.00565
	2	0.0029	0.00099	1	0.00114	0.00001	0.0031	10.1	0.000000175	0.00000019	6.1×10^{-7}	0.01	0.00025	0.00565
	3	0.0029	0.00099	1	0.00118	0.00001	0.0031	10.1	0.000000175	0.00000019	6.1×10^{-7}	0.01	0.00025	0.00565
3	**1**	0.0029	0.00099	1	0.0011	0.00001	0.0031	10.1	0.000000175	0.00000019	0.000061	0.01	0.00025	0.00565
	2	0.0029	0.00099	1	0.0011	0.00001	0.0031	10.1	0.000000175	0.00000019	0.00071	0.01	0.00025	0.00565
	3	0.0029	0.00099	1	0.0011	0.00001	0.0031	10.1	0.000000175	0.00000019	0.001361	0.01	0.00025	0.00565

3. Design Methodology

Predicting outcomes from datasets with labeled results is the goal of supervised machine learning, which is an area of artificial intelligence that describes a set of techniques and concepts for doing so. A powerful teaching technique that can be used to learn the method is an artificial neural network, which uses optimization to minimize error functions [45,46]. The network operating system is divided into two parts. The first part discusses the basic foundations of the RP-LMS dataset design, while the second part describes how to implement RP-LMS in the real world. Here, RP-LMS is used to numerically analyze the GAPF paradigm introduced by Equation (1). The suggested RP-LMS is introduced for multiple scenarios, with S-1 representing no change in fish numbers, S-2 showing an increase in planktonic populations due to increased CO_2 uptake, and S-3 showing a drop in fish numbers as a result of global warming. For the RP-LMS, the reference dataset is created using the Runge–Kutta technique and the NDSolver in Mathematica. For each variable with a range from 0 to 50, we provide 1251 discrete data points by maintaining a step size of 0.04. The collected information is then divided into three different datasets: one dataset is used for training (weight adjustment), one for validation (managing the learning process), and one for testing (evaluating the accuracy of the approximation). There is a predetermined number of observations in each dataset from which to calculate the optimal convergence rate.

To train the networks, the input vectors and target vectors have been arbitrarily split into three sets: 70% of the total dataset was used for training, 15% of the dataset was used to determine whether the network was generalizing and to halt training before the model became overfit, and 15% of the dataset was used to test the generalization of the network in a manner that was completely independent of the training. The number of layers, number of hidden neurons, learning process, and activation function employed in the experiment are all elaborated in the Table 4. Activation functions are the most important component of any deep learning neural network; they are primarily used to decide the outcome of deep learning techniques, their correctness, and the effectiveness of the training phase that can create or split a large-scale neural network. They determine whether to access or depress neurons in order to achieve the expected output depicted Figure 2. Since the neural network is sometimes trained with millions of data points, the activation function must be efficient and should reduce the time it takes to do a computation. The activation function used in this study is sigmoid function also called logistic function and can be calculated by

$$\sigma(\zeta) = \frac{1}{1 + e^{-z}} \tag{2}$$

where z is a real number and the number of nodes in a neural network hidden layer is calculated by

$$N = round(\frac{2 \times iN}{3} + oN), \tag{3}$$

where iN represents the number of input nodes and oN represents the number of output nodes. Additionally, as activation functions differ from one another, it is simple to apply back propagations and optimum techniques when measuring gradient loss functions in neural networks.

The architectures of artificial neural networks are shown in Figure 3. The GAPF model is trained multiple times to generate different results due to different initial conditions and samples. The neural network (RP-LMS) requires more memory but less time. Figure 4 shows the detailed flow chart for the design methodology. The mean squared discrepancy between output and objectives is referred to as mean square error. Lower numbers are preferable, while 0 indicates that there is no mistake. Table 4 lists all the important experimental details, such as the total number of layers, the total number of hidden neurons, and the activation function that will be used in the proposed study.

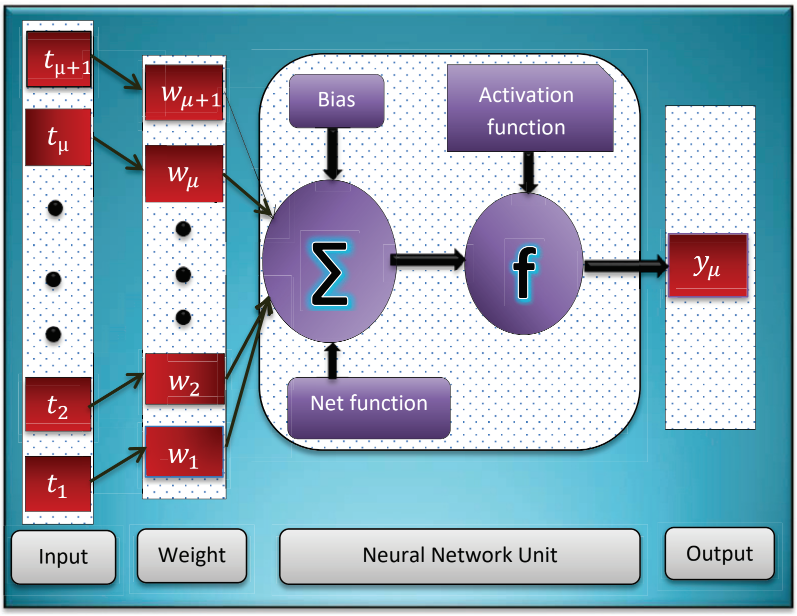

Figure 2. Architecture of artificial neural networks with single neuron.

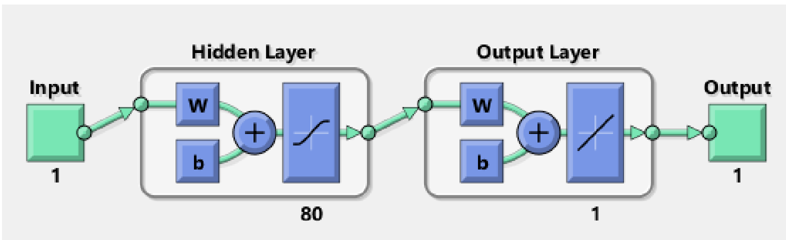

Figure 3. Neural networks architecture.

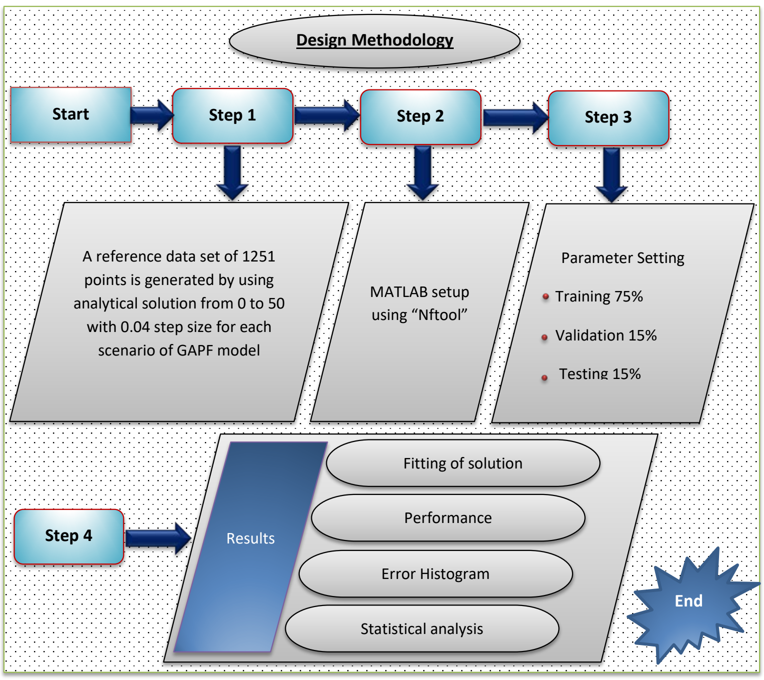

Figure 4. Flow chart for the design methodology.

Table 4. The dimensions and structure of the experiment's parameters.

Index	Description
Number of layers	Three
Layers structure	One input, one hidden, and one output layer
Hidden neurons	20–80
Training samples	875 samples
Testing samples	188 samples
Validation samples	188 sample
Learning methodology	Levenberg–Marquaradt Scheme
Label target data	Created with Adams numerical method
Maximum iteration	1000
Activation function	Sigmoid Symmetric Transfer Function

4. Discussion on Symmetry in Results

This section contains extensive scenario-based simulations, as well as a series of tables and graphs showing the validity and symmetry in the results of the suggested RP-LMS. Various examples of the GAPF model are constructed to evaluate the performance and efficiency of the design algorithm. The variance in different parameters and instances evaluated in the suggested model is shown in Table 5. The absorption ratio of GHGs by aquatic populations in seas (Δ_2) varies for various situations in the first scenario, while the average growth of the aquatic population (χ_1) due to CO_2 varies for three different scenarios in the second scenario. Similarly, the rate of global warming affecting fish populations (β_3) varies for different cases of study in Scenario (3). The fourth order Runge–Kutta solver in the MATHEMATICA programmer was used to carry out the numerical simulations of the Model (1). Rk4 obtains the input dataset for (RP-LMS) which ranges from 0 to 50 with a fixed time interval of 0.04. The dataset generates 1251 input points with 15% for validation, 70% for training, and 15% for users to test. The mean square error measures the average squared deviation from the goal value in relation to the outputs. Figure 5 demonstrates the best performance and symmetry for greenhouse gases and ambient temperature for scenario one, and the best validation performance is obtained only at epoch 7, where the values are (5.89×10^{-11} and 3.97×10^{-11}). On the other hand, Figure 6 demonstrates the best performance for the marine population and the fish community after eight iterations, and the performance obtained for both categories is 1.43×10^{-10} and 2.40×10^{-10}).

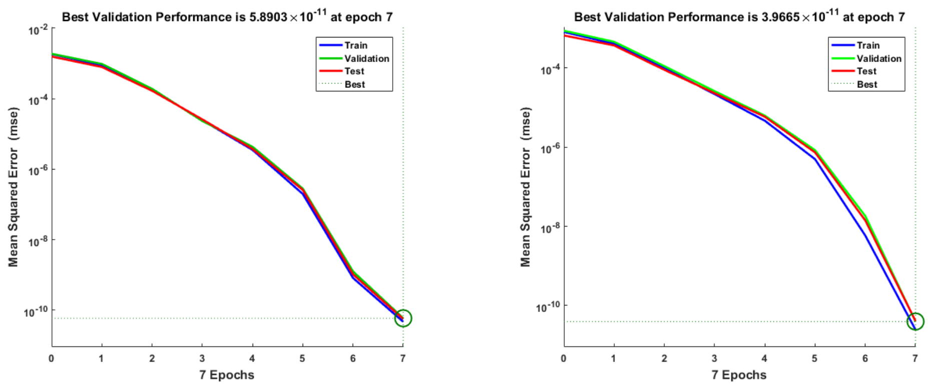

(**a**) (**b**)

Figure 5. Mean square error of RP-LMS through NNs for greenhouse gases and ambient temperature for Scenario 1. (**a**) **W(t)**; (**b**) **X(t)**.

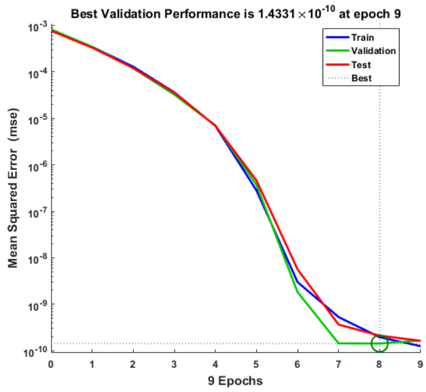

(**a**)

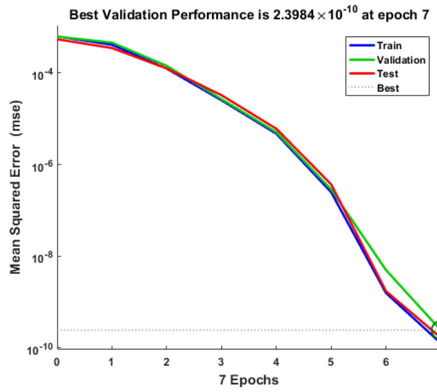

(**b**)

Figure 6. Mean square error of RP-LMS through NNs for aquatic population and fish population for Scenario 1. (**a**) **Y(t)**, (**b**) **Z(t)**.

Table 5. Numerical analysis of the RP-LMS in terms of mu, gradient, performance, and number of iterations for Scenarios 1 and 2.

Fitness on MSN										
Scenario	**Case Index**	**Neuron Setting**	**Training**	**Validation**	**Testing**	**Gradient**	**Performance**	**Mu**	**Epochs**	**R**
	w(t)	80	4.67×10^{-11}	5.89×10^{-11}	5.61×10^{-11}	4.36×10^{-9}	5.89×10^{-11}	1.00×10^{-10}	7	1
1	X(t)	80	5.61×10^{-11}	1.43×10^{-10}	2.12×10^{-10}	1.4817×10^{-8}	3.97×10^{-11}	1.00×10^{-10}	7	1
	Y(t)	80	3.11×10^{-13}	3.81×10^{-13}	3.42×10^{-13}	7.91×10^{-8}	1.43×10^{-10}	1.00×10^{-12}	9	1
	Z(t)	80	2.06×10^{-11}	2.10×10^{-11}	1.92×10^{-11}	4.4005×10^{-8}	2.40×10^{-10}	1.00×10^{-10}	7	1
	w(t)	45	4.09×10^{-11}	3.97×10^{-11}	2.45×10^{-11}	9.91×10^{-8}	3.81×10^{-13}	1.00×10^{-12}	234	1
2	X(t)	45	1.24×10^{-10}	2.40×10^{-10}	1.64×10^{-10}	9.98×10^{-8}	1.82×10^{-13}	1.00×10^{-12}	368	1
	Y(t)	45	1.61×10^{-13}	1.82×10^{-13}	1.87×10^{-13}	3.62×10^{-7}	2.10×10^{-11}	1.00×10^{-8}	1000	1
	Z(t)	45	6.29×10^{-13}	3.75×10^{-12}	1.54×10^{-12}	3.73×10^{-7}	3.75×10^{-12}	1.00×10^{-12}	1000	1

The best performance can be obtained for Scenario 2 by varying the average growth rate of the aquatic population, as shown in Figure 7. The highest performance results for greenhouse gases, atmospheric temperature, marine plankton, and fish community are (3.81×10^{-13}, 1.82×10^{-13}, 2.10×10^{-11}, 3.75×10^{-12}), respectively.

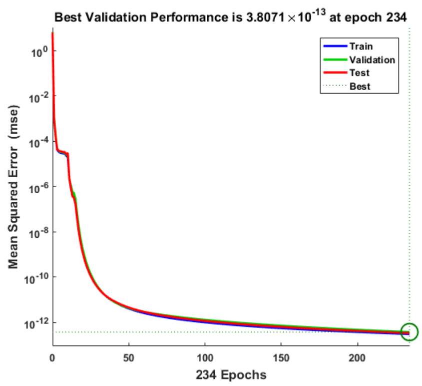

(**a**)

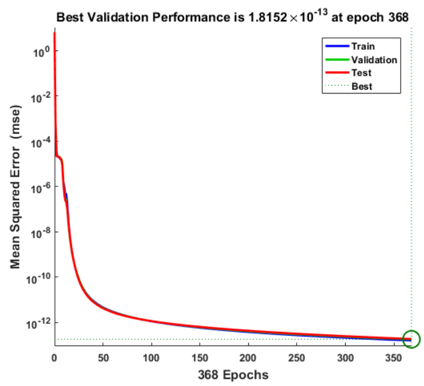

(**b**)

Figure 7. *Cont.*

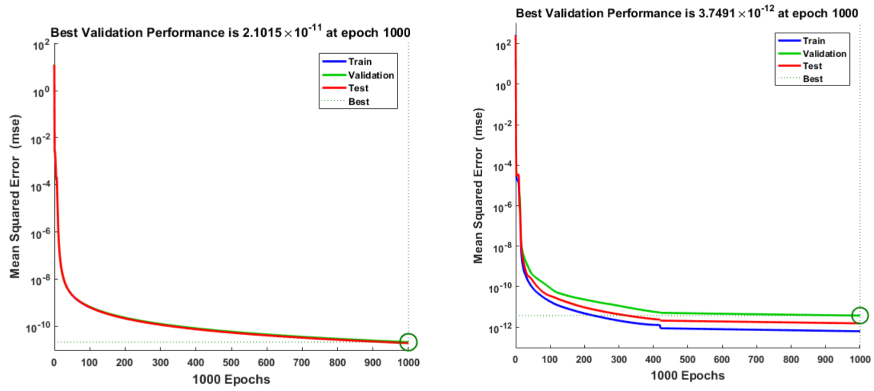

(**c**) (**d**)

Figure 7. Mean square error of RP-LMS through NNs for greenhouse gases, ambient temperature, aquatic population, and fish population for Scenario 2. (**a**) **W(t)**, (**b**) **X(t)**, (**c**) **Y(t)**, (**d**) **Z(t)**.

The proposed method has many parameters, such as mu, gradient, and many more. However, mu and gradient are the most well-known parameters. Mu is the part of the algorithm that controls how the neural network is trained. The choice of mu has a direct effect on the convergence of errors. In RP-LMS, mu depends on the maximum eigenvalue of the correlation matrix that was given as input. The default setting for the RP-LMS input value is 0.001, and its range is between 0.8 and 1. The outcomes of the RP-LMS through the supervised neural network for Scenario 1 in terms of mu, gradient, and validation checks for greenhouse gases, ambient temperature, aquatic population, and fish population are presented in Figure 8. By using only 7 to 10 iterations, the values for gradient are 4.36×10^{-9}, 1.49×10^{-8}, 7.91×10^{-8}, 4.405×10^{-8}; mu is 1×10^{-10}, 1×10^{-10}, 1×10^{-12}, 1×10^{-10}. In the same way, Figures 9 and 10 show the gradient and mu values for Scenario 2, which are 9.91×10^{-8}, 9.98×10^{-8}, 3.62×10^{-7}, 3.73×10^{-7} and 9.91×10^{-8}, 9.98×10^{-8}, 3.62×10^{-7}, 3.73×10^{-7}, respectively, at different numbers of iterations. The number of epochs can vary from 0 to 1000.

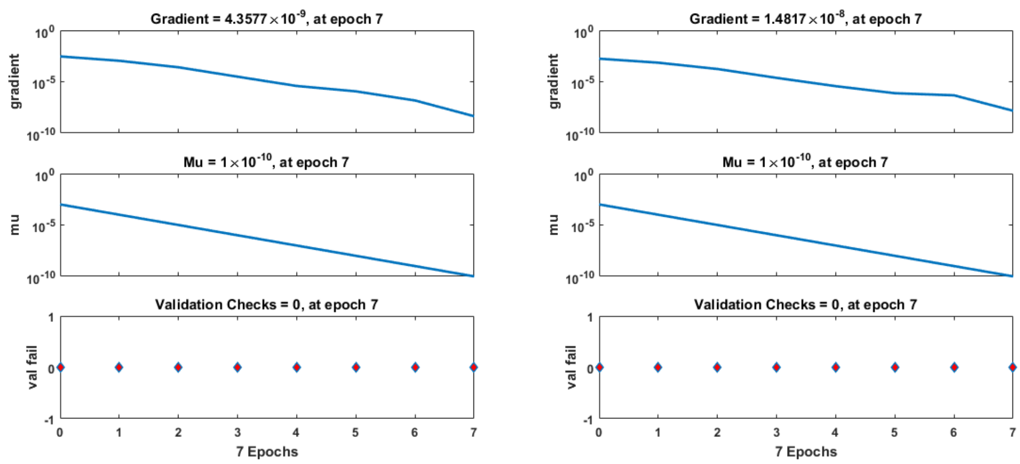

(**a**) (**b**)

Figure 8. *Cont.*

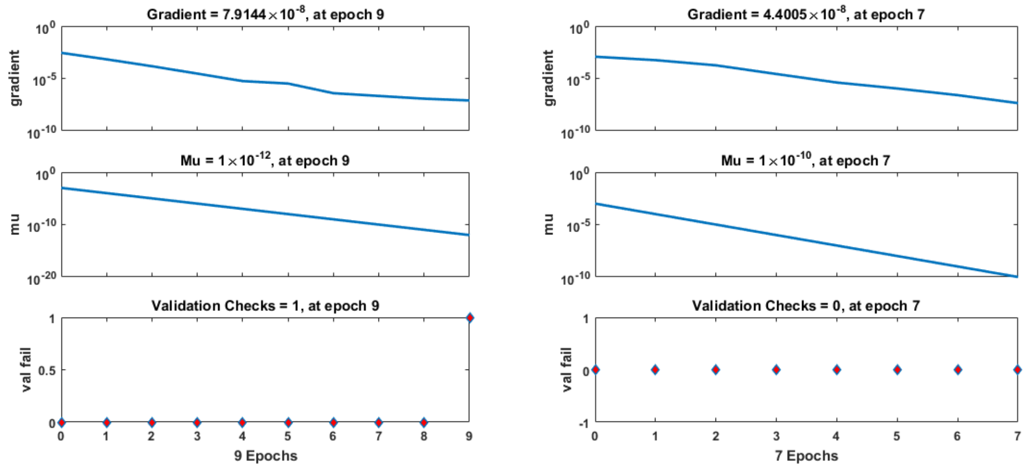

(**c**) (**d**)

Figure 8. Performance of RP-LMS through SNN in terms of mu, gradient, and validation checks for greenhouse gases, ambient temperature, aquatic population, and fish population for Case 1. (**a**) **W(t)**, (**b**) **X(t)**, (**c**) **Y(t)**, (**d**) **Z(t)**.

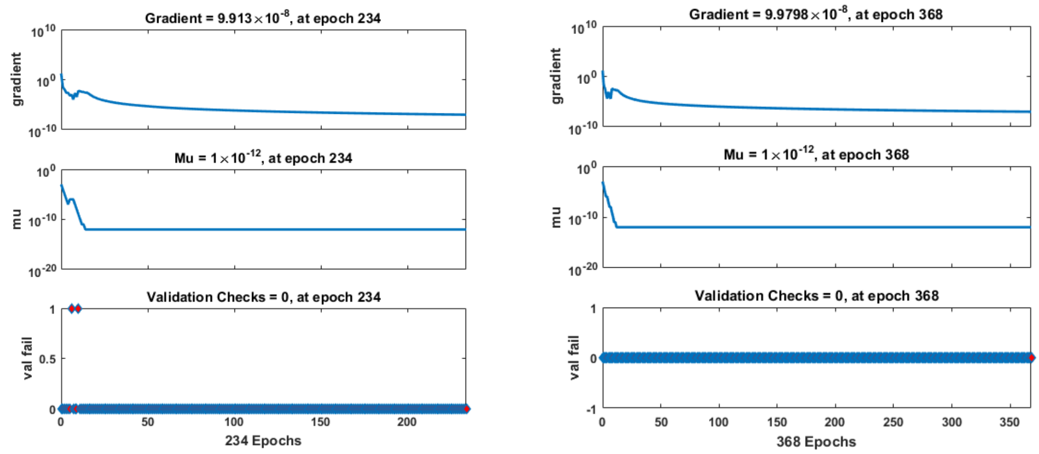

(**a**) (**b**)

Figure 9. Performance of RP-LMS through SNN in terms of mu, gradient, and validation checks for greenhouse gases and ambient temperature for Case 2. (**a**) **W(t)**, (**b**) **X(t)**.

Figures 11 and 12 show symmetric regression graphs of network outputs in relation to training, validation, and test set targets. The data must fall along a 45 degree line, where the network outputs are equal to the targets, for a perfect match. With R values of 0.95 or higher, the fit is acceptable for all datasets included in this problem. You can retrain the network by clicking Retrain in nftool if you need even more accurate results. This will alter the network's initial weights and biases, and it is possible that a retrained network will be better for it. In the GAPF model, the regression value is always 1. This shows that the proposed method is very effective. Moreover, for each scenario of the proposed model, we achieved a perfect surrogate model, as depicted on the lift side of Figures 9 and 10; this demonstrates that the methodology is more successful for data-driven real-world situations. Using RP-LMS, we can generate a proxy model for even the largest datasets.

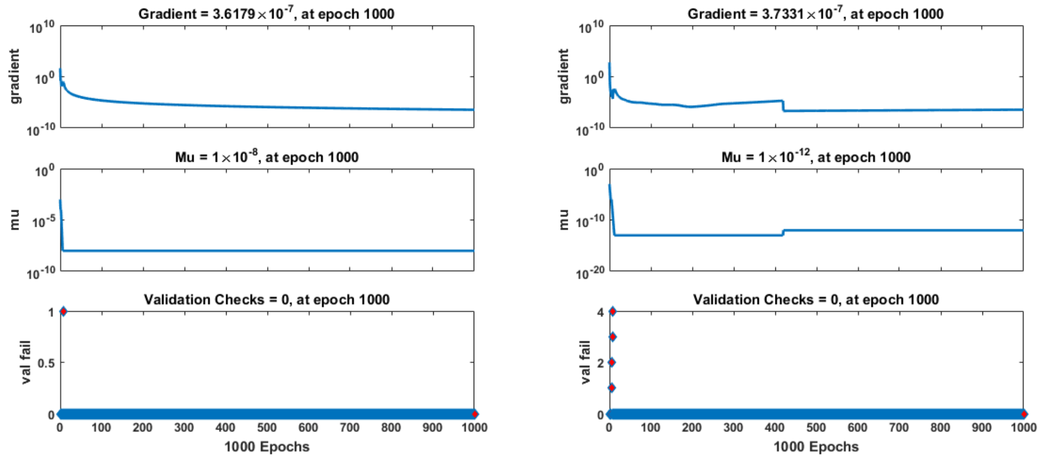

(**a**) (**b**)

Figure 10. Performance of RP-LMA through SNN in terms of mu, gradient, and validation checks for aquatic population, and fish population for Case 2. (**a**) **Y(t)**, (**b**) **Z(t)**.

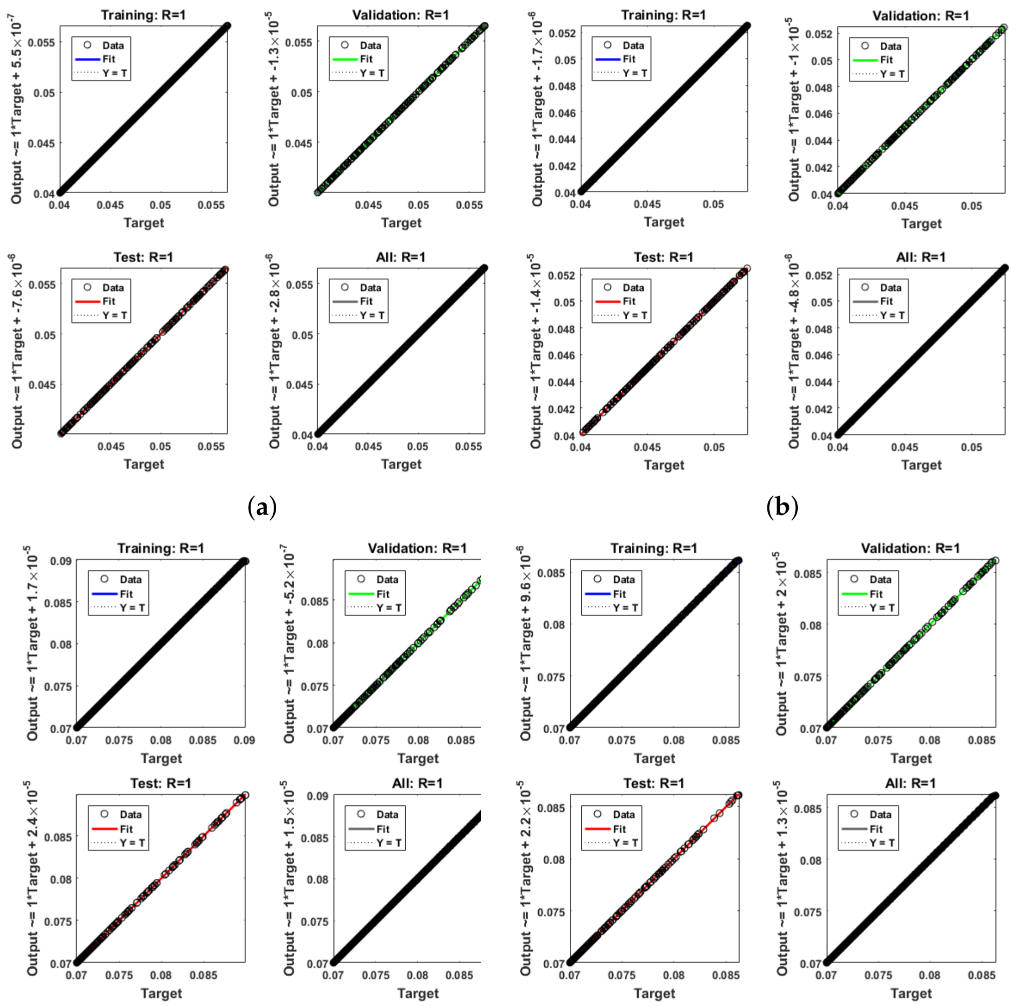

(**c**) (**d**)

Figure 11. Regression analysis of RP-LMS through SNN for training, validation, testing, and all samples, respectively, for the GAPF model in Case 1. (**a**) **W(t)**, (**b**) **X(t)**, (**c**) **Y(t)**, (**d**) **Z(t)**.

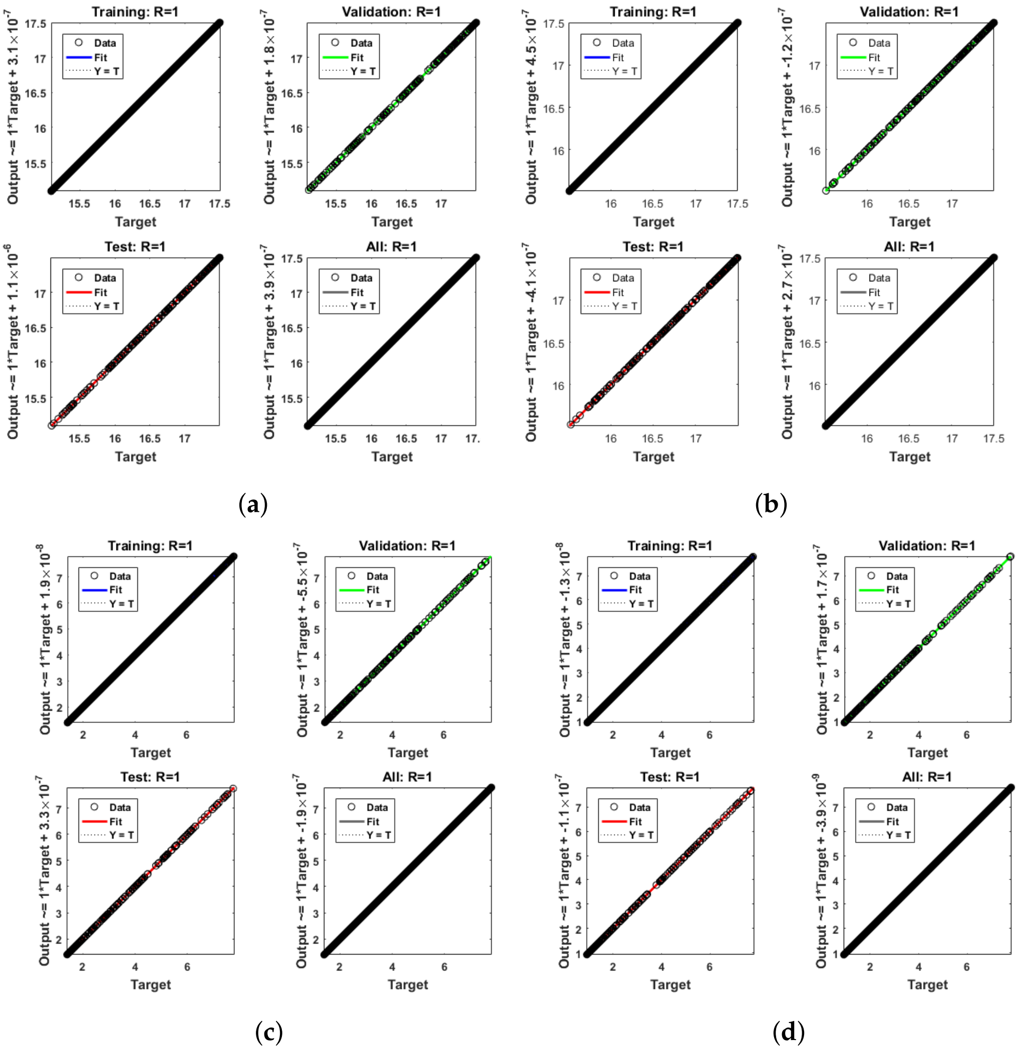

Figure 12. Regression analysis of RP-LMS through SNN for training, validation, testing, and all samples, respectively, for the GAPF model in Case 2. (**a**) **W(t)**, (**b**) **X(t)**, (**c**) **Y(t)**, (**d**) **Z(t)**.

The graphical analysis of the discussed methodology is further explained statistically in the following tables. Table 5 represents the detailed discussion of the proposed methodology for each scenario, such as the number of hidden neurons and the computation time taken for RP-LMS. Table 5 also shows the number of epochs for the proposed model in each scenario. Furthermore, it also explains the testing, validating, and performance data in each case. The numerical data for mu parameter, gradient, and regression is also discussed in the below table. Figure 13–15 shows the error histogram, and fitting graphs provide additional evidence of the effectiveness of the network. The training data is represented by the brown bars in Figure 13, the validation data is represented by the green bars, and the testing data is represented by the red bar. You can use the histogram to find outliers or data points where the fit is much worse than the rest of the data.

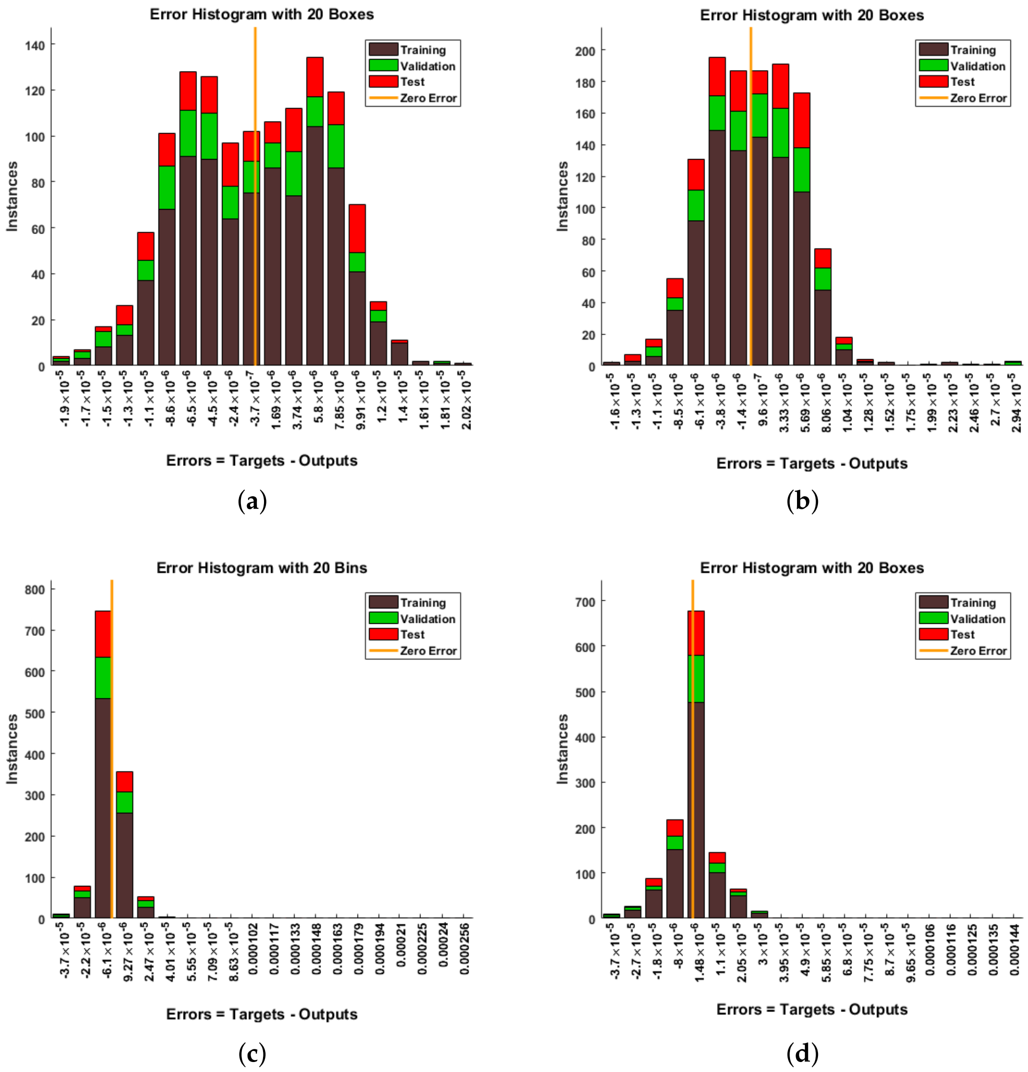

Figure 13. Error histogram for the proposed methodology in terms of greenhouse gases, ambient temperature, aquatic population, and fish population for Case Study 1. (**a**) **W(t)**, (**b**) **X(t)**, (**c**) **Y(t)**, (**d**) **Z(t)**.

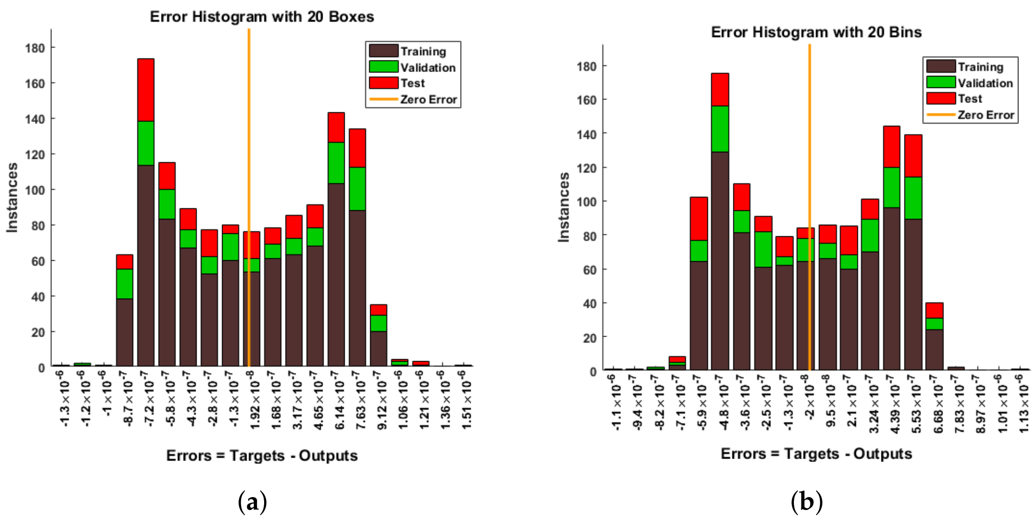

Figure 14. Error histogram for the proposed methodology in terms of greenhouse gases and ambient temperature for Case Study 2. (**a**) **W(t)**, (**b**) **X(t)**.

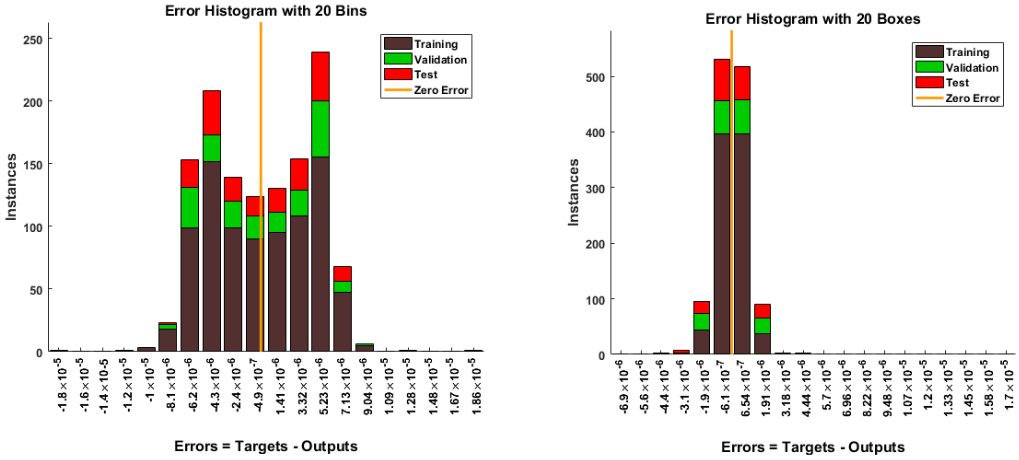

(**a**) (**b**)

Figure 15. Error histogram for the proposed methodology in terms of aquatic population and fish population for Case Study 2. (**a**) **Y(t)**, (**b**) **Z(t)**.

In addition, Figures 16–19 show a robust system behavior expected for the differential signaling of greenhouse gases with human plankton. The increase in greenhouse gas emissions is shown in the Figure 16. Figure 17 shows the increase in greenhouse gases due to the number of plankton contributing to the decrease in air temperature, and Figure 18 shows the increase in the population of plankton with increasing atmospheric pressure. On the other hand, as the females consume more plankton, their growth corresponds to the growth of the plankton populations. As plankton concentration increases to support CO_2 digestion, the number of fish in the total plankton diet increases, total O_2 digestion, and sea temperature decrease as shown in Figures 17 and 19. Tables 6–9 show statistical analysis of numerical solutions of the proposed methodology with the results obtained from a numerically solving model using "NDsolve" by varying a different number of parameters. The discussion also shows the error analysis of the comparative study.

Table 6. Statistical analysis of numerical solution and proposed methodology for varying GHG concentration through aquatic inhabitants in coral reefs, as well as error analysis for Greenhouse Gases.

	Δ_2 = 0.00101			Δ_2 = 0.00108			Δ_2 = 0.00114		
t	**RK4-W(t)**	**RP-LMS**	**Absolute Errors**	**RK4-W(t)**	**RP-LMS**	**Absoluten Errors**	**RK4-W(t)**	**RP-LMS**	**Absolute Errors**
0	0.04	0.040001	9.03×10^{-6}	0.04	0.039975	2.46×10^{-5}	0.04	0.04	4.69×10^{-6}
3.96	0.040976	0.040969	6.57×10^{-6}	0.040749	0.040753	4.19×10^{-6}	0.040468	0.040467	1.07×10^{-6}
7.96	0.041994	0.041987	6.89×10^{-6}	0.041528	0.04153	1.04×10^{-6}	0.040953	0.040954	1.08×10^{-6}
11.96	0.043052	0.043048	4.47×10^{-6}	0.042335	0.042332	2.96×10^{-6}	0.041454	0.041455	4.06×10^{-7}
15.96	0.044156	0.044153	2.97×10^{-6}	0.043174	0.043173	9.53×10^{-7}	0.041974	0.041972	1.98×10^{-6}
19.96	0.045312	0.045309	3.15×10^{-6}	0.044051	0.044057	6.90×10^{-6}	0.042517	0.042518	6.48×10^{-7}
23.96	0.04653	0.046531	1.78×10^{-6}	0.044971	0.044968	3.16×10^{-6}	0.043086	0.043089	3.24×10^{-6}
27.96	0.047816	0.047825	8.56×10^{-6}	0.045941	0.045937	4.35×10^{-6}	0.043685	0.043687	2.29×10^{-6}
31.96	0.049181	0.049189	7.98×10^{-6}	0.046968	0.046978	9.65×10^{-6}	0.044318	0.04432	2.31×10^{-6}
35.96	0.050633	0.050642	9.26×10^{-6}	0.048059	0.048063	3.67×10^{-6}	0.044989	0.044988	8.63×10^{-7}
39.96	0.052184	0.052187	3.20×10^{-6}	0.049222	0.049216	6.21×10^{-6}	0.045704	0.045706	1.98×10^{-6}
43.96	0.053845	0.053845	5.21×10^{-6}	0.050465	0.050469	3.65×10^{-6}	0.046466	0.046469	2.71×10^{-6}
47.96	0.055628	0.055624	4.63×10^{-6}	0.051798	0.051803	5.63×10^{-6}	0.047283	0.047284	1.28×10^{-6}
50	0.056589	0.056578	1.08×10^{-5}	0.052515	0.052517	2.28×10^{-6}	0.047722	0.04772	2.29×10^{-6}

Table 7. Statistical analysis of the numerical solution and the proposed methodology for varying the absorption probability of emission by aquatic inhabitants in seas, as well as the error analysis for ambient temperature, are presented.

	β_3 = 0.00061			β_3 = 0.000711			β_3 = 0.001361		
t	**RK4-X(t)**	**RP-LMS**	**Absolute Errors**	**RK4-X(t)**	**RP-LMS**	**Absolute Errors**	**RK4-X(t)**	**RP-LMS**	**Absolute Errors**
0	0.07	0.069998	1.61×10^{-6}	0.07	0.07003	2.96×10^{-5}	0.07	0.069876	0.000124
3.96	0.070063	0.070064	6.04×10^{-7}	0.070061	0.070061	4.44×10^{-7}	0.070059	0.070058	5.92×10^{-7}
7.96	0.070209	0.070208	1.10×10^{-6}	0.070195	0.070196	7.51×10^{-7}	0.070177	0.070179	2.08×10^{-6}
11.96	0.070483	0.070486	2.72×10^{-6}	0.070436	0.070437	2.28×10^{-7}	0.070377	0.070378	1.85×10^{-7}
15.96	0.070933	0.070932	1.04×10^{-6}	0.070822	0.07082	2.34×10^{-6}	0.070683	0.070679	3.30×10^{-6}
19.96	0.071607	0.071607	5.90×10^{-8}	0.071391	0.07139	9.44×10^{-7}	0.071117	0.071117	1.74×10^{-7}
23.96	0.072556	0.072555	3.47×10^{-7}	0.072181	0.072187	6.64×10^{-6}	0.071706	0.07171	4.05×10^{-6}
27.96	0.073834	0.07383	3.55×10^{-6}	0.073235	0.073232	3.07×10^{-6}	0.072478	0.072476	1.72×10^{-6}
31.96	0.075503	0.075507	4.80×10^{-6}	0.074602	0.074593	9.04×10^{-6}	0.073463	0.073458	4.69×10^{-6}
35.96	0.077632	0.077631	1.76×10^{-6}	0.076335	0.076353	1.77×10^{-5}	0.074694	0.074698	4.41×10^{-6}
39.96	0.080304	0.080302	2.12×10^{-6}	0.078495	0.07852	2.49×10^{-5}	0.076209	0.07622	1.15×10^{-5}
43.96	0.083614	0.083603	1.17×10^{-5}	0.081153	0.081124	2.88×10^{-5}	0.078051	0.078037	1.37×10^{-5}
47.96	0.087678	0.087703	2.53×10^{-5}	0.084393	0.084384	8.98×10^{-6}	0.08027	0.080262	8.05×10^{-6}
50	0.090085	0.089821	0.000264	0.086303	0.086154	0.000149	0.081565	0.081496	6.90×10^{-5}

Table 8. Statistical analysis of numerical solution and proposed methodology for varying aquatic rate of growth due to CO_2, as well as error analysis for aquatic population

	χ_1 = 0.00101			χ_1 = 0.00108			χ_1 = 0.00114		
t	**RK4-Y(t)**	**RP-LMS**	**Absolute Errors**	**RK4-Y(t)**	**RP-LMS**	**Absolute Errors**	**RK4-Y(t)**	**RP-LMS**	**Absolute Errors**
0	17.5	17.5	1.58×10^{-6}	17.5	17.5	1.18×10^{-6}	17.5	17.5	7.79×10^{-7}
3.96	17.46275	17.46275	6.97×10^{-7}	17.46603	17.46603	5.58×10^{-7}	17.47015	17.47015	2.35×10^{-7}
7.96	17.39636	17.39636	6.79×10^{-7}	17.40947	17.40947	3.79×10^{-7}	17.42596	17.42596	6.43×10^{-7}
11.96	17.30152	17.30152	3.77×10^{-7}	17.33074	17.33074	4.76×10^{-7}	17.36765	17.36765	5.78×10^{-7}
15.96	17.17871	17.1787	4.00×10^{-7}	17.23002	17.23002	2.45×10^{-7}	17.29512	17.29512	2.48×10^{-7}
19.96	17.02842	17.02842	4.90×10^{-7}	17.10746	17.10746	6.59×10^{-7}	17.20828	17.20828	2.91×10^{-7}
23.96	16.8512	16.8512	6.22×10^{-7}	16.96324	16.96324	6.17×10^{-7}	17.10699	17.10699	1.04×10^{-7}
27.96	16.64766	16.64766	5.26×10^{-7}	16.79754	16.79754	2.25×10^{-7}	16.9911	16.9911	4.06×10^{-11}
31.96	16.41845	16.41845	2.25×10^{-7}	16.61057	16.61056	6.34×10^{-7}	16.86044	16.86044	4.60×10^{-7}
35.96	16.16432	16.16432	7.46×10^{-7}	16.40255	16.40255	5.56×10^{-8}	16.71482	16.71482	3.60×10^{-7}
39.96	15.88609	15.88609	4.01×10^{-7}	16.17379	16.17379	3.62×10^{-7}	16.55409	16.55409	5.06×10^{-7}
43.96	15.5847	15.5847	6.51×10^{-8}	15.92463	15.92463	9.43×10^{-8}	16.37806	16.37806	4.10×10^{-7}
47.96	15.26118	15.26118	6.81×10^{-7}	15.6555	15.6555	4.45×10^{-7}	16.18659	16.18659	5.13×10^{-7}
50	15.08803	15.08803	1.39×10^{-6}	15.51071	15.51071	1.11×10^{-6}	16.08296	16.08296	1.00×10^{-6}

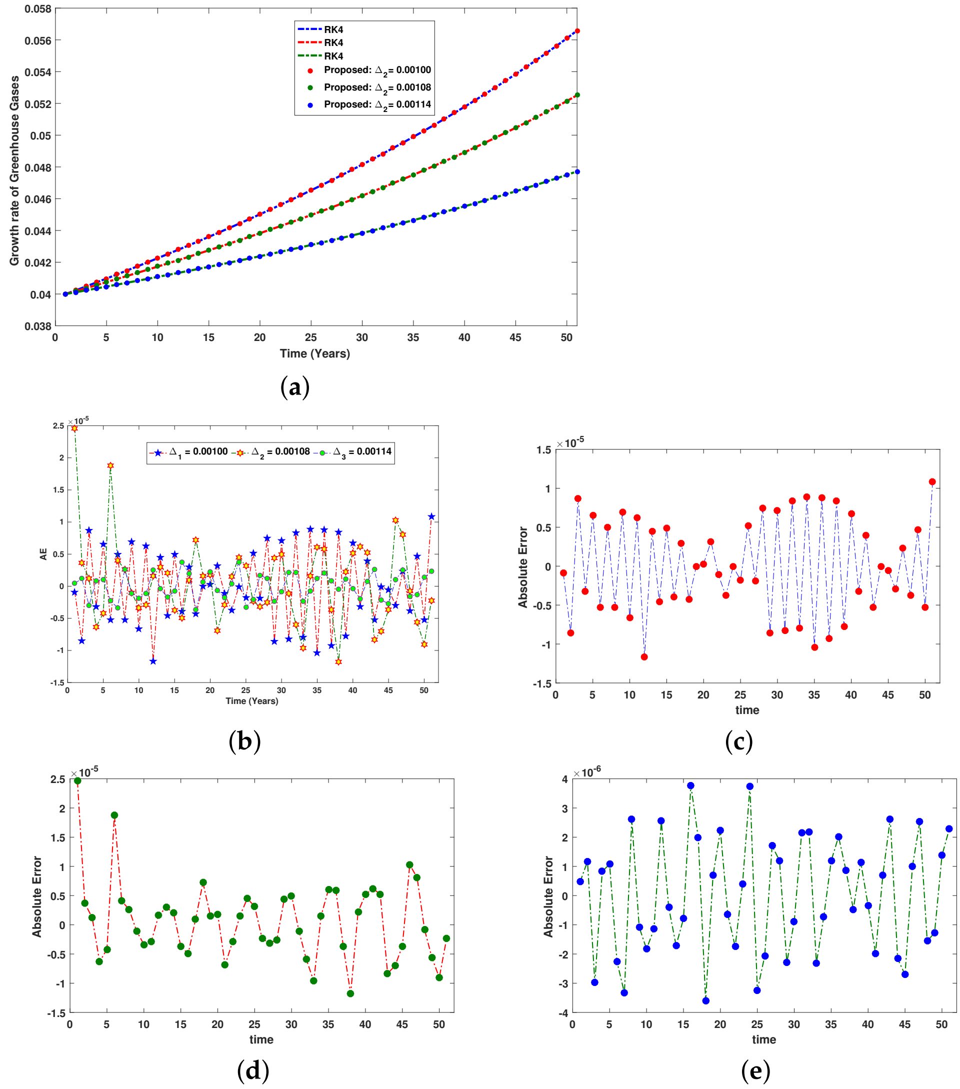

Figure 16. Comparison between the numerical reference solution and the proposed RP-LMS through SNN for greenhouse gases. (**a**) **Impact of** Δ_2 **on greenhouse gases**, (**b**) **collective analysis of Absolute Error**, (**c**) **analysis of case 1's errors**, (**d**) **analysis of case 2's errors**, (**e**) **analysis of case 3's errors**.

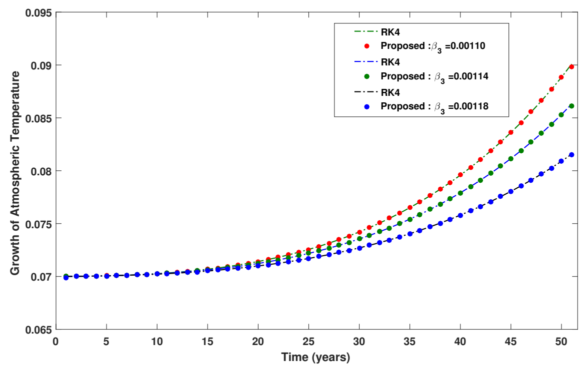

(**a**)

Figure 17. *Cont.*

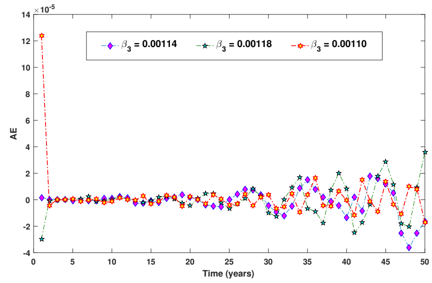

(**b**)

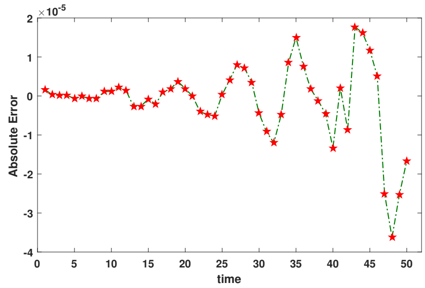

(**c**)

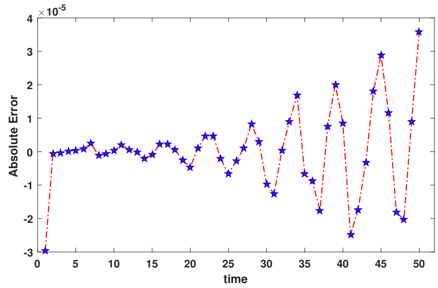

(**d**)

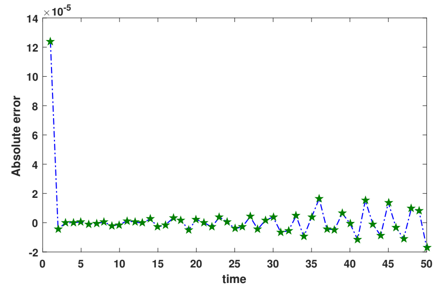

(**e**)

Figure 17. Comparison between the numerical reference solution and the proposed RP-LMS through SNN for ambient temperature. (**a**) **Impact of** β_3 **on atmospheric temperature**, (**b**) **collective analysis of Absolute Error,** (**c**) **analysis of case 1's errors**, (**d**) **analysis of case 2's errors**, (**e**) **analysis of case 3's errors**.

Table 9. Statistical analysis of numerical solution and the proposed methodology for varying hampering rate of fish populations by global warming and also show the error analysis for fish population.

	β_3 = 0.00101			β_3 = 0.001361			β_3 = 0.00071		
t	**RK4-Z(t)**	**RP-LMS**	**Absolute Error**	**RK4-Z(t)**	**RP-LMS**	**Absolute Error**	**RK4-Z(t)**	**RP-LMS**	**Absolute Error**
0	7.8	7.79998	1.95×10^{-5}	7.8	7.799982	1.77×10^{-5}	7.8	7.8	4.53×10^{-7}
3.96	6.586341	6.58634	6.31×10^{-7}	6.22928	6.229279	1.41×10^{-6}	7.057025	7.057025	2.74×10^{-7}
7.96	5.553165	5.553169	4.72×10^{-6}	4.966141	4.966142	1.03×10^{-6}	6.378245	6.378246	1.05×10^{-7}
11.96	4.687032	4.687033	5.13×10^{-7}	3.967926	3.967924	2.17×10^{-6}	5.765623	5.765623	3.40×10^{-7}
15.96	3.96571	3.965706	3.45×10^{-6}	3.185818	3.185819	7.15×10^{-7}	5.214275	5.214275	8.22×10^{-8}
19.96	3.369767	3.369771	4.14×10^{-6}	2.578881	2.578882	9.97×10^{-7}	4.719984	4.719985	3.02×10^{-7}
23.96	2.881718	2.881713	4.86×10^{-6}	2.112426	2.112426	3.76×10^{-7}	4.278938	4.278939	3.05×10^{-7}
27.96	2.485687	2.485692	5.11×10^{-6}	1.757278	1.757278	3.88×10^{-7}	3.887535	3.887535	3.45×10^{-9}
31.96	2.167335	2.167331	4.85×10^{-6}	1.489318	1.489318	7.67×10^{-7}	3.542271	3.542271	5.84×10^{-8}
35.96	1.913895	1.9139	5.90×10^{-6}	1.289007	1.289007	2.60×10^{-7}	3.239676	3.239676	4.26×10^{-9}
39.96	1.71418	1.714177	2.61×10^{-6}	1.140805	1.140804	4.41×10^{-7}	2.976299	2.976299	2.42×10^{-7}
43.96	1.558555	1.558548	7.45×10^{-6}	1.032519	1.03252	1.02×10^{-6}	2.748719	2.74872	1.76×10^{-7}
47.96	1.438823	1.438821	2.42×10^{-6}	0.954651	0.95465	9.05×10^{-7}	2.553575	2.553575	2.23×10^{-7}
50	1.389308	1.389327	1.86×10^{-5}	0.924196	0.924203	7.54×10^{-6}	2.465482	2.465494	1.17×10^{-5}

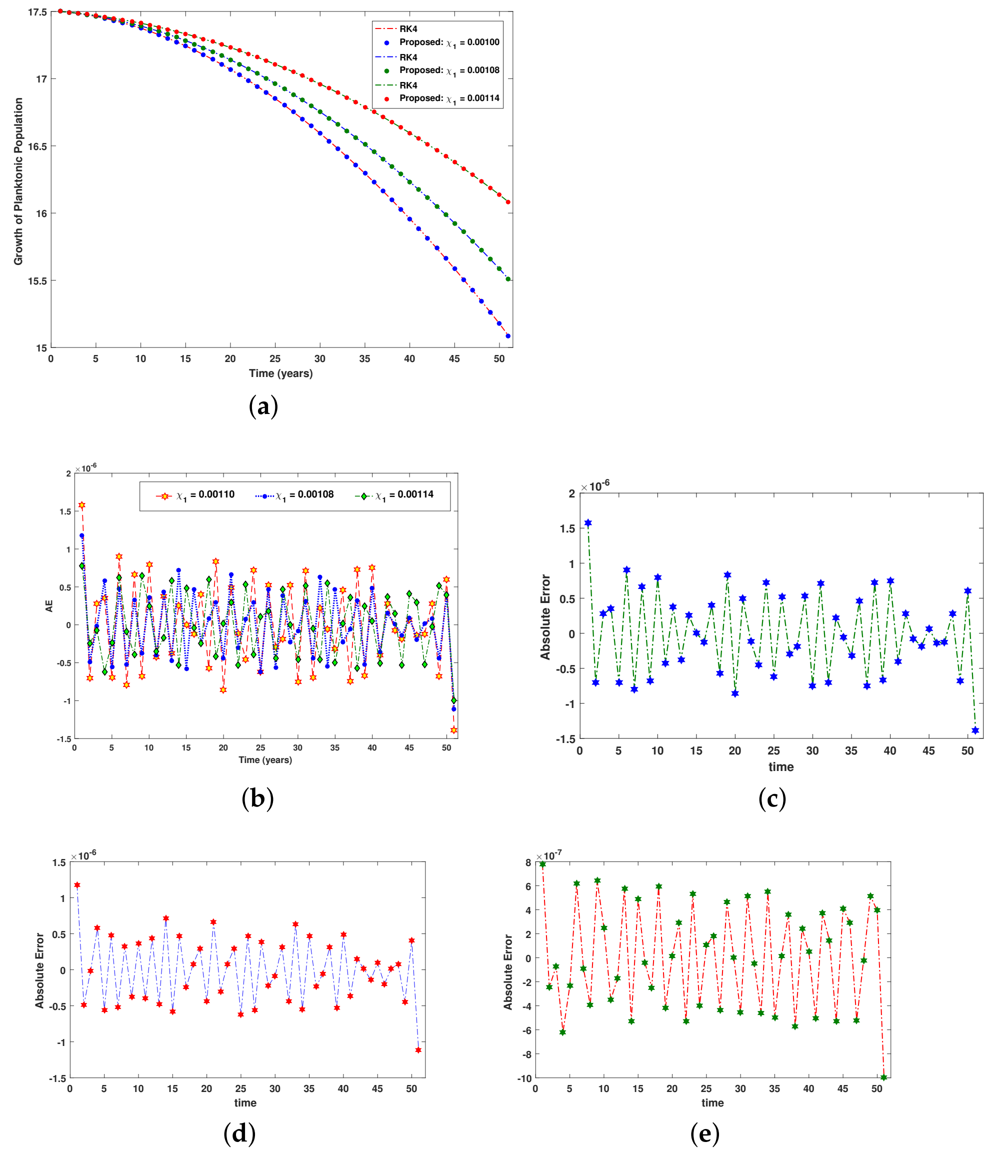

Figure 18. Comparison between the numerical reference solution and the proposed RP-LMS through SNN for aquatic population. (**a**) **Impact of** χ_1 **on planktonic population**, (**b**) **collective analysis of Absolute Error**, (**c**) **analysis of case 1's errors**, (**d**) **analysis of case 2's errors**, (**e**) **analysis of case 3's errors**.

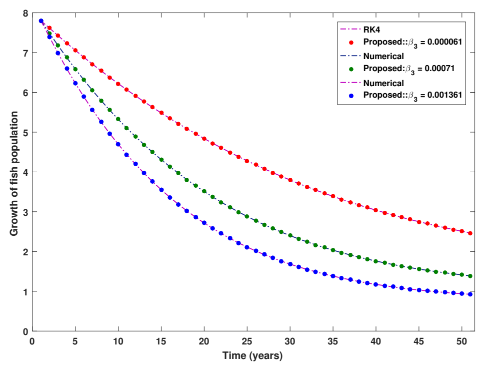

(**a**)

Figure 19. *Cont.*

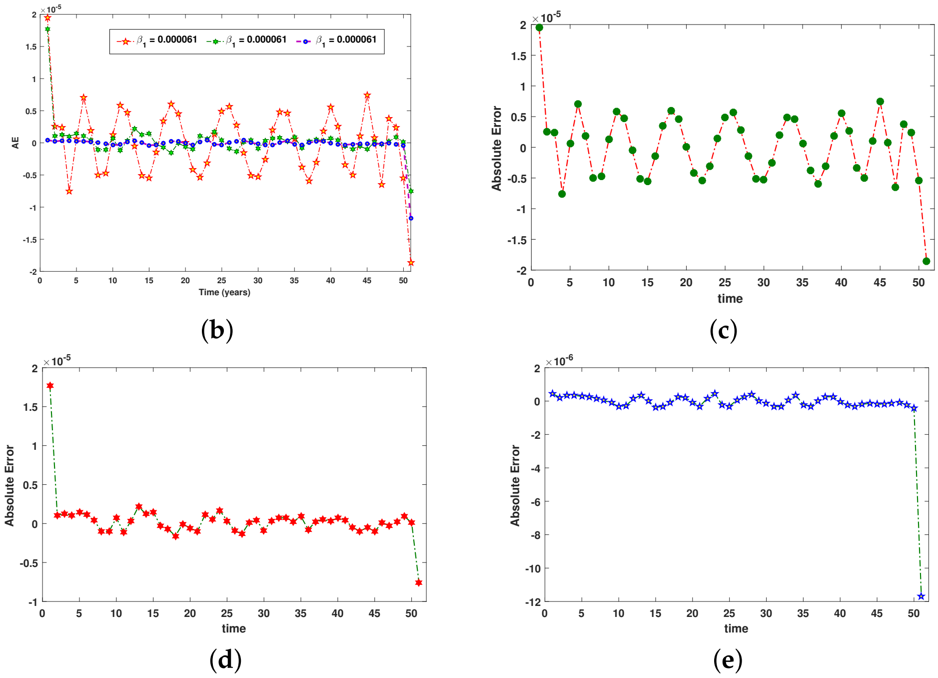

Figure 19. Comparison between the numerical reference solution and the proposed RP-LMS through SNN for fish population. (**a**) **Impact of** β_3 **on fish population**, (**b**) **collective analysis of Absolute Error**, (**c**) **analyze of error for case 1**, (**d**) **analyze of error for case 2**, (**e**) **analyze of error for case 3**.

5. Conclusions

This paper examined the nonlinear ordinary differential equation with an initial condition related to an environmental management model, where greenhouse gases, environmental temperature, plankton population, and fish population are considered as parameters. To study the environmental management model, a hybridized technique based on reverse propagation through a supervised neural network was designed. The solutions obtained by RP-LMS exhibited better symmetry in terms of results obtained and have taken less time and produced a more accurate result compared to the RK4 numerical technique. In addition, the graphical and statistical approaches confirm the stability and symmetry of the design algorithm. We have used graphical and statistical methods to study how changes in the concentration of greenhouse gases (GHGs) affect aquatic ecosystems and global warming. Furthermore, if current trends continue, aquatic organisms will be transformed into conservation lands within the next fifty years due to the ongoing decline in plankton variability and marine resources. In this work, we solve the real-world challenge associated with the system of nonlinear differential equations. Partial differential equations and fractional order differential equations are two real-world problems that can be tackled with this method in the future. In addition, the scope of artificial neural networks can be easily broadened to address problems in other systems where traditional methods have failed, including quick forest plantations, optimum control schemes, fluid dynamics issues (such as the removal of dyes from water), and many others.

Author Contributions: All authors contributed equally to this paper. All authors have read and agreed to the published version of the manuscript.

Funding: The study was funded by the Deanship of Scientific Research at Umm Al-Qura University, Makkah, Saudi Arabia (Grant Code: 20UQU0067DSR); and Researchers Supporting Project (TURSP-2020/107), Taif University, Taif, Saudi Arabia.

Institutional Review Board Statement: Not applicable.

Informed Consent Statement: Not applicable.

Data Availability Statement: The data related to this study is available from the corresponding author upon reasonable request.

Acknowledgments: The authors would like to thank the Deanship of Scientific Research at Umm Al-Qura University for supporting this work by Grant Code: (20UQU0067DSR); and Researchers Supporting Project number (TURSP-2020/107), Taif University, Taif, Saudi Arabia.

Conflicts of Interest: The authors declare no conflict of interest.

Abbreviations

The following abbreviations are used in this manuscript:

Abbreviation	Description
ANNs	Artificial Neural Networks
RP	Reverse Propagated
LMS	Levenberg–Marquaradt Scheme
G	Greenhouse Gases
A	Atmospheric Temperature
P	Planktonic Population
F	Fish Population
NN	Neural Network
NODEs	Nonlinear Ordinary Differential Equations
MSE	Mean Square Error
GHGs	Greenhouse Gases
Deqs	Differential Equations
FFN	Feed Forward Network
MQE	Mean Quadratic Error
CO_2	Carbon dioxide gas
O_2	Oxygen gas

References

1. Mandal, S.; Islam, M.S.; Biswas, M.H.A.; Akter, S. A mathematical model applied to investigate the potential impact of global warming on marine ecosystems. *Appl. Math. Model.* **2022**, *101*, 19–37. [CrossRef]
2. Lüthi, D.; Le Floch, M.; Bereiter, B.; Blunier, T.; Barnola, J.M.; Siegenthaler, U.; Raynaud, D.; Jouzel, J.; Fischer, H.; Kawamura, K.; et al. High-resolution carbon dioxide concentration record 650,000–800,000 years before present. *Nature* **2008**, *453*, 379–382. [CrossRef] [PubMed]
3. Change, I.C. *The Physical Science Basis*; Working Group I Contribution to the Fifth Assessment Report of the Intergovernmental Panel on Climate Change; World Meteorological Organization: Geneva, Switzerland, 2013.
4. Beardall, J.; Stojkovic, S.; Larsen, S. Living in a high CO_2 world: Impacts of global climate change on marine phytoplankton. *Plant Ecol. Divers.* **2009**, *2*, 191–205. [CrossRef]
5. Sherman, E.; Moore, J.K.; Primeau, F.; Tanouye, D. Temperature influence on phytoplankton community growth rates. *Glob. Biogeochem. Cycles* **2016**, *30*, 550–559. [CrossRef]
6. Gomiero, A.; Bellerby, R.; Zeichen, M.M.; Babbini, L.; Viarengo, A. Biological responses of two marine organisms of ecological relevance to on-going ocean acidification and global warming. *Environ. Pollut.* **2018**, *236*, 60–70. [CrossRef] [PubMed]
7. Cooley, S.R.; Bello, B.; Bodansky, D.; Mansell, A.; Merkl, A.; Purvis, N.; Ruffo, S.; Taraska, G.; Zivian, A.; Leonard, G.H. Overlooked ocean strategies to address climate change. *Glob. Environ. Change* **2019**, *59*, 101968. [CrossRef]
8. Speers, A.E.; Besedin, E.Y.; Palardy, J.E.; Moore, C. Impacts of climate change and ocean acidification on coral reef fisheries: An integrated ecological–economic model. *Ecol. Econ.* **2016**, *128*, 33–43. [CrossRef]
9. Roxy, M.K.; Modi, A.; Murtugudde, R.; Valsala, V.; Panickal, S.; Prasanna Kumar, S.; Ravichandran, M.; Vichi, M.; Lévy, M. A reduction in marine primary productivity driven by rapid warming over the tropical Indian Ocean. *Geophys. Res. Lett.* **2016**, *43*, 826–833. [CrossRef]
10. Asch, R.G.; Cheung, W.W.; Reygondeau, G. Future marine ecosystem drivers, biodiversity, and fisheries maximum catch potential in Pacific Island countries and territories under climate change. *Mar. Policy* **2018**, *88*, 285–294. [CrossRef]
11. Ma, S.; Liu, Y.; Li, J.; Fu, C.; Ye, Z.; Sun, P.; Yu, H.; Cheng, J.; Tian, Y. Climate-induced long-term variations in ecosystem structure and atmosphere-ocean-ecosystem processes in the Yellow Sea and East China Sea. *Prog. Oceanogr.* **2019**, *175*, 183–197. [CrossRef]
12. Talloni-Álvarez, N.E.; Sumaila, U.R.; Le Billon, P.; Cheung, W.W. Climate change impact on Canada's Pacific marine ecosystem: The current state of knowledge. *Mar. Policy* **2019**, *104*, 163–176. [CrossRef]
13. Sekerci, Y.; Petrovskii, S. Mathematical modelling of plankton–oxygen dynamics under the climate change. *Bull. Math. Biol.* **2015**, *77*, 2325–2353. [CrossRef] [PubMed]

14. Rana, T.; Imran, M.A.; Baz, A. A Component Model with Verifiable Composition for the Construction of Emergency Management Systems. *Arab. J. Sci. Eng.* **2020**, *12*, 10683–10692. [CrossRef]
15. Barange, M.; Merino, G.; Blanchard, J.; Scholtens, J.; Harle, J.; Allison, E.; Allen, J.; Holt, J.; Jennings, S. Impacts of climate change on marine ecosystem production in societies dependent on fisheries. *Nat. Clim. Change* **2014**, *4*, 211–216. [CrossRef]
16. Mandal, S.; Islam, M.; Biswas, M.; Ali, H. Modeling the potential impact of climate change on living beings near coastal areas. *Model. Earth Syst. Environ.* **2021**, *7*, 1783–1796. [CrossRef]
17. Le Quéré, C.; Moriarty, R.; Andrew, R.M.; Canadell, J.G.; Sitch, S.; Korsbakken, J.I.; Zeng, N.; Schuster, U.; Schwinger, J.; Tilbrook, B.; et al. Global Carbon Budget 2015. *Earth Syst. Sci. Data* **2015**, *7*, 349–396. [CrossRef]
18. Häder, D.P.; Barnes, P.W. Comparing the impacts of climate change on the responses and linkages between terrestrial and aquatic ecosystems. *Sci. Total Environ.* **2019**, *682*, 239–246. [CrossRef] [PubMed]
19. Baltar, F.; Bayer, B.; Bednarsek, N.; Deppeler, S.; Escribano, R.; Gonzalez, C.E.; Hansman, R.L.; Mishra, R.K.; Moran, M.A.; Repeta, D.J.; et al. Towards integrating evolution, metabolism, and climate change studies of marine ecosystems. *Trends Ecol. Evol.* **2019**, *34*, 1022–1033. [CrossRef]
20. McLean, M.; Mouillot, D.; Lindegren, M.; Engelhard, G.; Villéger, S.; Marchal, P.; Brind'Amour, A.; Auber, A. A climate-driven functional inversion of connected marine ecosystems. *Curr. Biol.* **2018**, *28*, 3654–3660. [CrossRef]
21. Ben-Hasan, A.; Christensen, V. Vulnerability of the marine ecosystem to climate change impacts in the Arabian Gulf—An urgent need for more research. *Glob. Ecol. Conserv.* **2019**, *17*, e00556. [CrossRef]
22. Doney, S.C.; Ruckelshaus, M.; Emmett Duffy, J.; Barry, J.P.; Chan, F.; English, C.A.; Galindo, H.M.; Grebmeier, J.M.; Hollowed, A.B.; Knowlton, N.; et al. Climate change impacts on marine ecosystems. *Annu. Rev. Mar. Sci.* **2012**, *4*, 11–37. [CrossRef] [PubMed]
23. Chapman, E.J.; Byron, C.J.; Lasley-Rasher, R.; Lipsky, C.; Stevens, J.R.; Peters, R. Effects of climate change on coastal ecosystem food webs: Implications for aquaculture. *Mar. Environ. Res.* **2020**, *162*, 105103. [CrossRef] [PubMed]
24. Fabien, M.; Laure, V.; Philippe, V.; Nicolas, B.; Caroline, U.; Pierluigi, C.; Antonio, E.; Follesa, M.C.; Michele, G.; Angélique, J.; et al. Capturing the big picture of Mediterranean marine biodiversity with an end-to-end model of climate and fishing impacts. *Prog. Oceanogr.* **2019**, *178*, 102179.
25. Hinners, J.; Hense, I.; Kremp, A. Modelling phytoplankton adaptation to global warming based on resurrection experiments. *Ecol. Model.* **2019**, *400*, 27–33. [CrossRef]
26. Kumar, R.; Baz, A.; Alhakami, H.; Alhakami,W.; Agrawal, A.; Khan, R.A. A hybrid fuzzy rule-based multi-criteria framework for sustainable-security assessment of web application. *Ain Shams Eng. J.* **2021**, *2*, 2227–2240. [CrossRef]
27. Cao, L. Artificial intelligence in retail: Applications and value creation logics. *Int. J. Retail. Distrib. Manag.* **2021**, *49*. [CrossRef]
28. Tian, Y. Artificial intelligence image recognition method based on convolutional neural network algorithm. *IEEE Access* **2020**, *8*, 125731–125744. [CrossRef]
29. Zhao, S.; Blaabjerg, F.; Wang, H. An overview of artificial intelligence applications for power electronics. *IEEE Trans. Power Electron.* **2020**, *36*, 4633–4658. [CrossRef]
30. Li, H.; Wu, P.; Zeng, N.; Liu, Y.; Alsaadi, F.E. A survey on parameter identification, state estimation and data analytics for lateral flow immunoassay: From systems science perspective. *Int. J. Syst. Sci.* **2022**, 1–21. [CrossRef]
31. Dohn, N.B.; Kafai, Y.; Mørch, A.; Ragni, M. Survey: Artificial Intelligence, Computational Thinking and Learning. *KI-Künstliche Intell.* **2022**, *36*, 5–16. [CrossRef]
32. Khan, N.A.; Alshammari, F.S.; Romero, C.A.T.; Sulaiman, M. Study of Nonlinear Models of Oscillatory Systems by Applying an Intelligent Computational Technique. *Entropy* **2021**, *23*, 1685. [CrossRef] [PubMed]
33. Khan, N.A.; Alshammari, F.S.; Romero, C.A.T.; Sulaiman, M.; Mirjalili, S. An Optimistic Solver for the Mathematical Model of the Flow of Johnson Segalman Fluid on the Surface of an Infinitely Long Vertical Cylinder. *Materials* **2021**, *14*, 7798. [CrossRef] [PubMed]
34. Khan, N.A.; Ibrahim Khalaf, O.; Andrés Tavera Romero, C.; Sulaiman, M.; Bakar, M.A. Application of Intelligent Paradigm through Neural Networks for Numerical Solution of Multiorder Fractional Differential Equations. *Comput. Intell. Neurosci.* **2022**, *2022*, 2710576. [CrossRef] [PubMed]
35. Khan, N.A.; Sulaiman, M.; Tavera Romero, C.A.; Laouini, G.; Alshammari, F.S. Study of Rolling Motion of Ships in Random Beam Seas with Nonlinear Restoring Moment and Damping Effects Using Neuroevolutionary Technique. *Materials* **2022**, *15*, 674. [CrossRef] [PubMed]
36. Ganie, A.H.; Fazal, F.; Tavera Romero, C.A.; Sulaiman, M. Quantitative Features Analysis of Water Carrying Nanoparticles of Alumina over a Uniform Surface. *Nanomaterials* **2022**, *12*, 878. [CrossRef] [PubMed]
37. Khan, M.F.; Sulaiman, M.; Romero, C.A.T.; Alshammari, F.S. A quantitative study of non-linear convective heat transfer model by novel hybrid heuristic driven neural soft computing. *IEEE Access* **2022**, *10*, 34133–34153. [CrossRef]
38. Rahman, I.U.; Sulaiman, M.; Alarfaj, F.K.; Kumam, P.; Laouini, G. Investigation of Non-Linear MHD Jeffery–Hamel Blood Flow Model Using a Hybrid Metaheuristic Approach. *IEEE Access* **2021**, *9*, 163214–163232. [CrossRef]
39. Fawad Khan, M.; Bonyah, E.; Alshammari, F.S.; Ghufran, S.M.; Sulaiman, M. Modelling and Analysis of Virotherapy of Cancer Using an Efficient Hybrid Soft Computing Procedure. *Complexity* **2022**, *2022*, 9660746. [CrossRef]
40. Baz, A.; Alhakami, H.; Alshareef, E. A framework of computational model for predicting the spread of COVID-19 pandemic in Saudi Arabia. *Int. J. Intell. Eng. Syst.* **2020**, *13*, 463–475. [CrossRef]

41. Bukhari, A.H.; Raja, M.A.Z.; Sulaiman, M.; Islam, S.; Shoaib, M.; Kumam, P. Fractional neuro-sequential ARFIMA-LSTM for financial market forecasting. *IEEE Access* **2020**, *8*, 71326–71338. [CrossRef]
42. Ara, A.; Khan, N.A.; Razzaq, O.A.; Hameed, T.; Raja, M.A.Z. Wavelets optimization method for evaluation of fractional partial differential equations: An application to financial modelling. *Adv. Differ. Equ.* **2018**, *2018*, 8. [CrossRef]
43. Khan, N.A.; Sulaiman, M.; Aljohani, A.J.; Bakar, M.A. Mathematical models of CBSC over wireless channels and their analysis by using the LeNN-WOA-NM algorithm. *Eng. Appl. Artif. Intell.* **2022**, *107*, 104537. [CrossRef]
44. Khan, I.; Raja, M.A.Z.; Shoaib, M.; Kumam, P.; Alrabaiah, H.; Shah, Z.; Islam, S. Design of neural network with Levenberg-Marquardt and Bayesian regularization backpropagation for solving pantograph delay differential equations. *IEEE Access* **2020**, *8*, 137918–137933. [CrossRef]
45. Alghamdi, H.; Alsubait, T.; Alhakami, H.; Baz, A. A review of optimization algorithms for university timetable scheduling. *Eng. Technol. Appl. Sci. Res.* **2020**, *10*, 6410–6417. [CrossRef]
46. Iqbal, A.; Raza, M.S.; Ibrahim, M.; Baz, A.; Alhakami, H.; Saeed, M.A. An Improved Approach for Finding Rough Set Based Dynamic Reducts. *IEEE Access* **2020**, *08*, 173008–173023. [CrossRef]